catalysts

MDPI

Article

Effect of Morphology on the Photoelectrochemical Activity of TiO_2 Self-Organized Nanotube Arrays

Houda Ennaceri [1,*], Kristina Fischer [1], Kevin Hanus [1], Abdelkrim Chemseddine [2], Andrea Prager [1], Jan Griebel [1], Mathias Kühnert [1], Agnes Schulze [1] and Bernd Abel [1]

[1] Department Functional Surfaces, Leibniz-Institute of Surface Engineering (IOM), Permoserstraße 15, 04318 Leipzig, Germany; kristina.fischer@iom-leipzig.de (K.F.); kevin.hanus@iom-leipzig.de (K.H.); andrea.prager@iom-leipzig.de (A.P.); jan.griebel@iom-leipzig.de (J.G.); mathias.kuehnert@iom-leipzig.de (M.K.); agnes.schulze@iom-leipzig.de (A.S.); bernd.abel@iom-leipzig.de (B.A.)

[2] Institute of Solar Fuels, Helmholtz-Zentrum Berlin für Materialien und Energie, Hahn-Meitner-Platz 1, 14109 Berlin, Germany; chemseddine@helmholtz-berlin.de

* Correspondence: houda.ennaceri@iom-leipzig.de

Received: 8 November 2019; Accepted: 19 February 2020; Published: 1 March 2020

Abstract: In the present work, highly ordered titanium dioxide (TiO_2) nanotube anodes were grown using a rapid anodization process. The photoelectrochemical performances of these electrodes strongly depend on the anodization conditions. Parameters such as electrolyte composition, anodization potential and anodization time are shown to affect the geometrical parameters of TiO_2 nanotubes. The optimal anodization parameters are determined by photocurrent measurements, linear sweep voltammetry and electrochemical impedance spectroscopy. The thickness of the tube wall and its homogeneity is shown to strongly depend on the anodization potential, and the formation mechanism is discussed. This study permits the optimization of the photocurrent density and contributes to further improvement of the photoelectrochemical water-splitting performance of TiO_2 nanotube photoelectrodes.

Keywords: TiO_2 nanotubes; electrochemical anodization; electrochemical impedance spectroscopy; photoelectrochemical properties

1. Introduction

Since the revolutionary report by Fujishima and Honda in 1972 [1] on water splitting into oxygen and hydrogen using a TiO_2 electrode, rigorous research has been devoted to hydrogen production through solar water-splitting processes. Other semiconducting materials, such as bismuth vanadate ($BiVO_4$), hematite (α-Fe_2O_3), tungsten trioxide (WO_3), and tantalum (oxy) nitrides (TaON) are reported to show high efficiencies towards photoelectrochemical (PEC) water splitting [2–5]. In recent years, research groups have been developing heterostructures like $BiVO_4/TiO_2$ [6,7] or $WO_3/BiVO_4$ [8] for efficient photoelectrochemical water splitting. In these studies, TiO_2 or WO_3 nanorods provide direct conduction pathways, minimizing recombination of photogenerated charge carriers. In the case of TiO_2, these nanotube or nanorod arrays, with their high surface area, provide a practical solution for building photoreactors for water purification and an alternative to titania powder or dense films [9]. Therefore, 3D titanium dioxide nanotube structures have attracted tremendous attention due to their uniform morphologies, large surface area and controllable size, as well as their potential applications, such as photo catalysis [10], dye sensitized solar cells [11], self-cleaning surfaces [12], corrosion resistance [13], wastewater treatment [14], biomedical implants [15], gas sensing [16] and solar hydrogen production [17,18].

Different approaches have been used for the synthesis of TiO_2 nanotubular structures, such as atomic layer deposition (ALD) [19], hydrothermal synthesis [20], and electrochemical anodization [21].

The growth of TiO_2 nanotubes by ALD requires the use of nanoporous templates, such as anodic aluminum oxide. This template-assisted requirement limits the choice of substrates and requires post-processing in order to separate the TiO_2 nanotubes from the template, in which the as-prepared TiO_2 nanotube arrays may break [22]. On the other hand, the hydrothermal synthesis technique consists of the hydrothermal treatment of titanium dioxide solutions followed by post-annealing treatment, and results in the non-ordered distribution of the TiO_2 nanotubes [23]. Among these methods, the electrochemical anodization route is widely investigated, and has attracted great interest since the growth of the very first highly ordered titanium dioxide by Zwilling et al. in 1999 [24,25]. Electrochemical anodization is a facile method to prepare functional materials on metal substrates, and enables us to synthesize highly self-organized structures at ambient temperature.

The functional properties of TiO_2 nanotubes are related to different parameters, such as the crystal structure and surface morphology, which are dependent on the preparation parameters.

It is reported in the literature that the nanotube diameter increases with a higher anodization voltage [26]. Previous work by Smith et al. reported that TiO_2 nanotubes with large diameters exhibit a better photocatalytic activity because the catalyst's surface is more exposed [27]. Another study by Mazzarolo et al. [28] reported the effect of the top morphology of the tubes on their corresponding photocatalytic activity, while other researchers have focused their research on the effect of tube length on the photocatalytic properties of TiO_2 nanotubes [29].

In this work, highly ordered and self-organized TiO_2 nanotube arrays were fabricated using a rapid anodization process. A series of TiO_2 nanotubes were prepared under different anodization potentials, electrolyte compositions and anodization times. The effects of the varying anodization parameters on the TiO_2 nanotube's geometrical parameters, as well as their photoelectrochemical properties, were investigated.

2. Results and Discussion

2.1. Formation Mechanism of TiO_2 Nanotubes

The formation of TiO_2 Nano tubular structures is a complex process, and the mechanisms are still controversial [30,31]. Previous works have discussed the formation mechanisms of TiO_2 nanotubes based on the field-assisted dissolution theory (FAD) [32], which suggests that the reaction happening at the anode is the oxidation of the titanium metal, releasing Ti^{4+} and electrons (Equation (1)). The Ti^{4+} ions then react with the OH^- and O^{2-} provided by the water, leading to the formation of titanium hydroxide (Equation (3)) and titanium oxide (Equation (4)).

$$Ti \rightarrow Ti^{4+} + 4e^- \quad (1)$$

$$Ti^{4+} + 4OH^- \rightarrow Ti(OH)_4 \quad (2)$$

$$Ti^{4+} + 2O^{2-} \rightarrow TiO_2 \quad (3)$$

$$Ti(OH)_4 \rightarrow TiO_2 + 2H_2O \quad (4)$$

Simultaneously, and under the effect of the electric field, the fluoride ions (F^-) in the electrolyte migrate to the anode, and the formed hydroxide layer or compact TiO_2 layer subsequently dissolves into $[TiF_6]^{2-}$ under the corrosion effect (Equations (5) and (6)).

$$TiO_2 + 6F^- + 4h^+ \rightarrow [TiF_6]^{2-} + H_2O \quad (5)$$

$$Ti(OH)_4 + 6F^- \rightarrow [TiF_6]^{2-} + 4OH^- \quad (6)$$

$[TiF_6]^{2-}$ is soluble in the electrolyte, which results in the formation of a large number of cracks on the surface of compact layer (as illustrated in Figure 1). As the reactions continue, the cracks gradually turn into nanotubes. The TiO_2 nanotubes' growth at the Ti/TiO_2 interface and the TiO_2 dissolution at

the TiO_2/electrolyte interface are two competitive processes, which highly depend on the anodization parameters. The TiO_2 nanotubes reach a steady growth rate when the Ti anodization rate and the TiO_2 dissolution rate become equal.

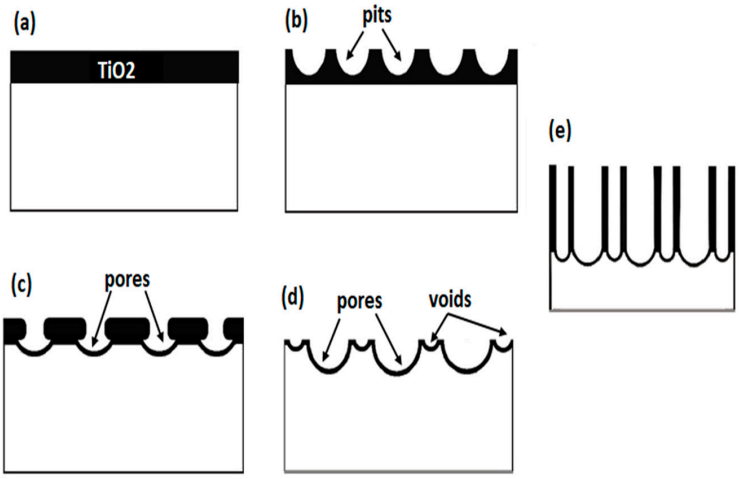

Figure 1. Formation mechanism of TiO_2 nanotubes (**a**) formation of TiO2 compact layer (**b**–**d**) formation of cracks on the surface of the compact layer (**e**) steady growth of TiO2 nanotubes.

2.2. Chemical Composition

The surface crystal structure of the samples was investigated using X-ray diffraction as illustrated in Figure 2a. The as-anodized samples show two diffraction peaks located at 38.30° and 40.20°, corresponding to the (002) and (101) crystallographic planes of metallic titanium (Joint Committee on Powder Diffraction Standards (JCPDS) Card No. 44-1294). The as-anodized samples were post-annealed nanotubes at 420 °C for 90 min, with heating and cooling rates of 10 K per minute. The XRD pattern of the post-annealed nanotubes is dominated by the (004) plane. In addition, the diffraction peaks located at 2θ = 25.366°, 37.85°, 38.41°, 48.00°, 51.6°, 54.00°, 54.99°, 62.93°, 68.75°, 70.84°, 75.00°, and 76.19°, correspond to the (100), (004), (112), (200), (202), (105), (211), (213), (116), (220), (215), and (301) planes of the tetragonal anatase phase of titanium dioxide (JCPDS Card No. 21-1272). Figure 2 refers to the TiO_2 nanotubes anodized at 30 V for 30 min using a 0.8 wt% ammonium fluoride concentration.

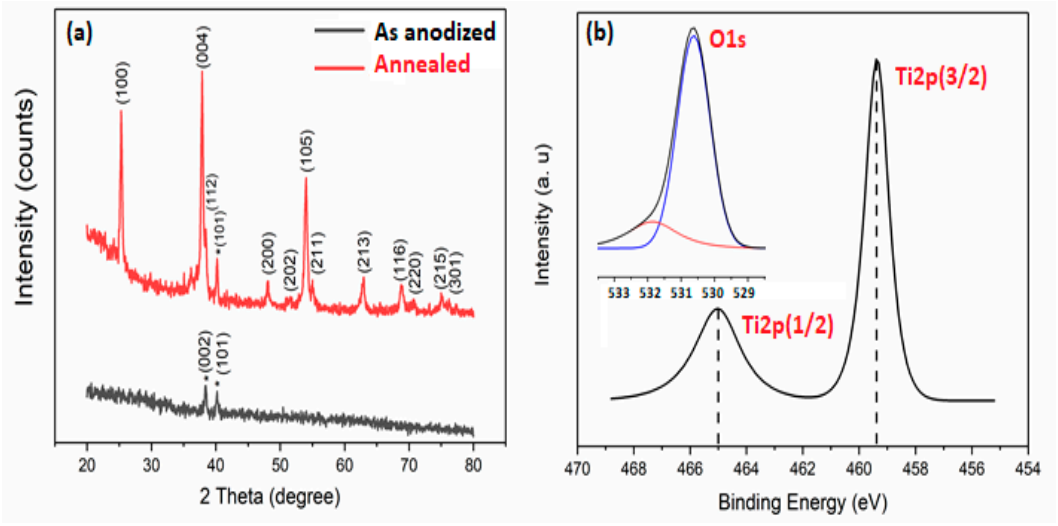

Figure 2. (**a**) X-ray diffraction pattern of the as-anodized and post-annealed TiO_2 nanotubes (**b**) X-ray photoelectron spectra of the Ti2p (inset shows the O1s region of the TiO_2 nanotube).

An X-ray photoelectron spectroscopy (XPS) study was performed in order to elucidate the composition of the fabricated titanium dioxide nanotubes (see Figure 2b). The peaks obtained from XPS analysis show well-resolved Ti2p (3/2) and Ti2p (1/2) peaks located at 459.36 eV and 465.02 eV, respectively, indicating Ti^{4+} (Figure 2b). On the other hand, the peaks located at 530.62 eV and 531.85 eV indicate the O1s peaks (inset of Figure 2b). The first peak located at 530.62 eV is characteristic of Ti and O in TiO_2, on the other hand, the O1s peak located at 531.85 eV is attributed to the hydroxyl groups on the outermost TiO_2 surface as well as the adsorbed water resulting from moisture adsorption in air.

2.3. Electrical Response during the Anodization Process

In this work, a series of TiO_2 nanotubes were prepared under different anodization potentials, different electrolyte concentrations and with different anodization times. Figure 3 shows the current–time curve recorded by the Rigol Digital Multimeter during the anodization of titanium foil in the ethylene glycol electrolytes with different ammonium fluoride concentrations, varying from 0.4 to 1.2 wt%. The anodization potential (30V) and time (30 min) were kept constant for all samples.

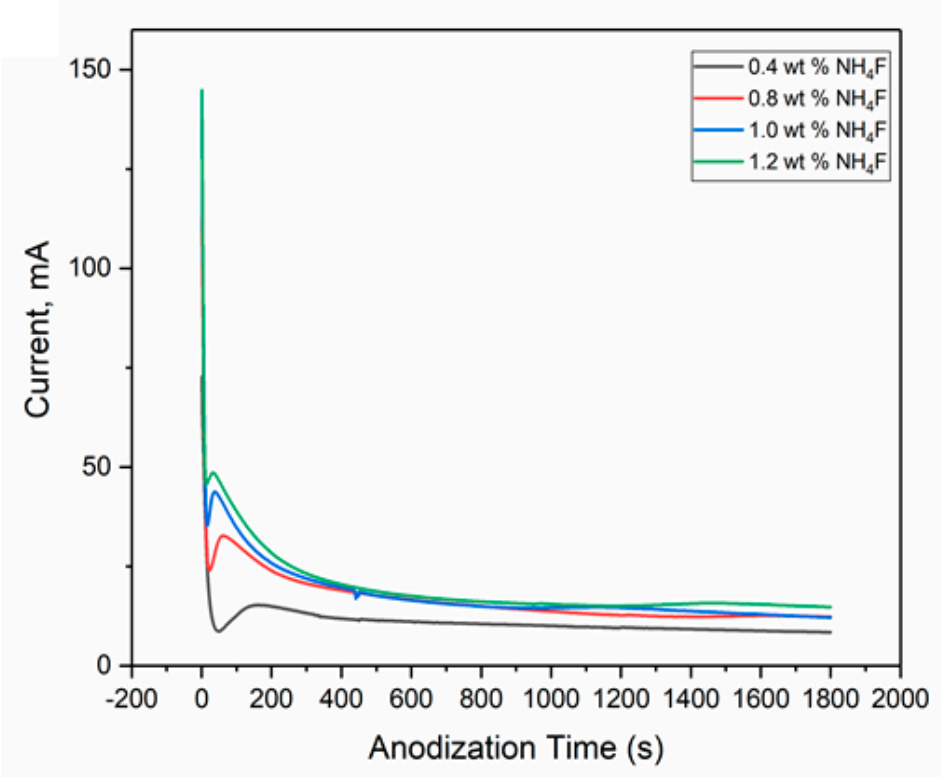

Figure 3. Current–time response during the anodization process using different electrolyte concentrations (anodization time: 30 min, anodization voltage: 30 V).

As shown in Figure 3, the anodization current is at its maximum value at the beginning of the anodization process, after which a rapid decrease is observed, which is due to the formation of a compact TiO_2 layer on the surface of the titanium substrate (Figure 1a). According to Ohm's law, the resistance of the compact layer is directly proportional to its thickness, which explains the first portion of the current–time response curve (Figure 3), showing a downward trend as the compact film thickness increases. The second portion of the current–time response curve shows an increase in the anodization current, which is explained by the formation of TiO_2 pores/embryos (Figure 1b–d), which gradually and slowly grow into self-organized nano-tubular morphology (Figure 1e). The last stage of the anodization process shows the steady state growth of TiO_2 nanotubes, which is achieved when the titanium electrochemical oxidation and TiO_2 dissolution rates become equal, reaching dynamic equilibrium.

2.4. Photoelectrochemical Testing (PEC)

2.4.1. Effect of Electrolyte Concentration

The current–transient curves of the TiO_2, prepared using different electrolyte concentrations under solar illumination (solar simulator), are illustrated in Figure 4.

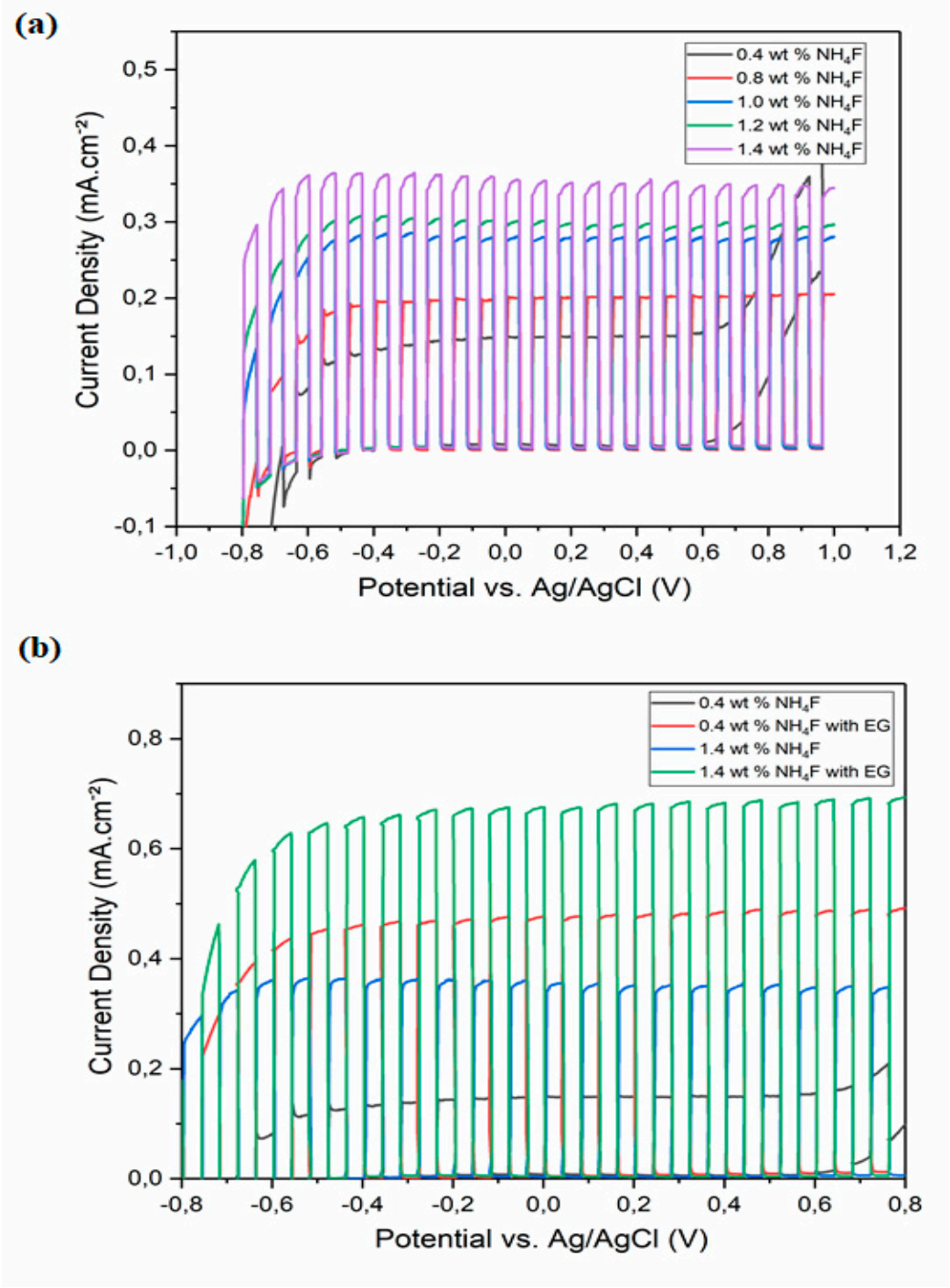

Figure 4. Current transient of the TiO_2 nanotubes prepared using different ammonium fluoride concentrations (**a**) without ethylene glycol (**b**) with ethylene glycol added (samples prepared using constant anodization time (30 min) and anodization voltage (30 V), annealed at 420 °C for 90 min).

It can be observed that the photocurrent density increases with an increasing amount of ammonium fluoride in the electrolyte solution (Figure 5a). In fact, a higher ammonium fluoride concentration enhances the electric field intensity and therefore increases the etching rate during anodization. In addition, 10 vol% of ethylene glycol as a hole scavenger in the KOH solution is shown to almost double the photocurrent density, and enhances the charge separation and carrier lifetime. The lowest photocurrent density is observed for TiO_2 nanotubes with the smallest pore diameter (lowest concentration of ammonium fluoride), which prevents the electrolyte from diffusing into the tubes, leading to a decrease in the photocurrent density.

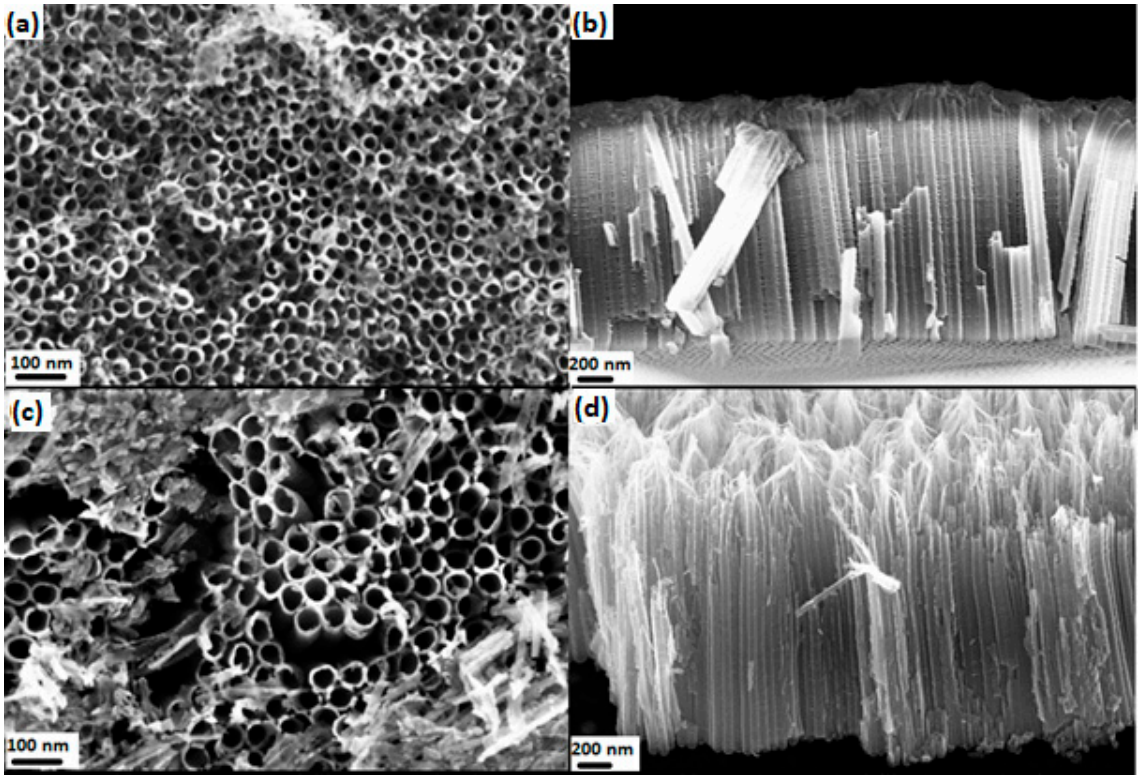

Figure 5. Surface and cross-section images of the TiO_2 nanotubes prepared using different ammonium fluoride concentrations (**a**,**b**) 0.4 wt% NH_4F (**c**,**d**) 1.4 wt% NH_4F (constant anodization time (30 min) and anodization voltage (30 V)).

Moreover, according to the SEM images, the tube length was not affected by the ammonium fluoride concentration, and the series of prepared TiO_2 nanotubes had an average tube length of 1.7 μm. However, the pore diameter is shown to increase with higher ammonium fluoride concentrations. The average pore diameter was calculated from the SEM top view images and showed a clear variation when changing the electrolyte ammonium fluoride concentration, but keeping the other parameters constant. The pore diameter is shown to increase from 33 to 58 nm, with increasing ammonium fluoride concentrations from 0.4 to 1.4 wt%. The TiO_2 nanotubes with higher opening exhibited a higher photocurrent density (Figure 4). The increase in the pore opening makes the electrolyte solution diffuse easily in the tubes, resulting in an improved photoelectrochemical activity.

2.4.2. Effect of Anodization Time

The tube length increased with longer anodization times, with 1.7, 2.1 and 2.9 μm for 30, 60 and 90 min, respectively. This increase in the tube length is illustrated in Figure 6a–c. The pore opening size remained constant at 53 nm under different anodization times.

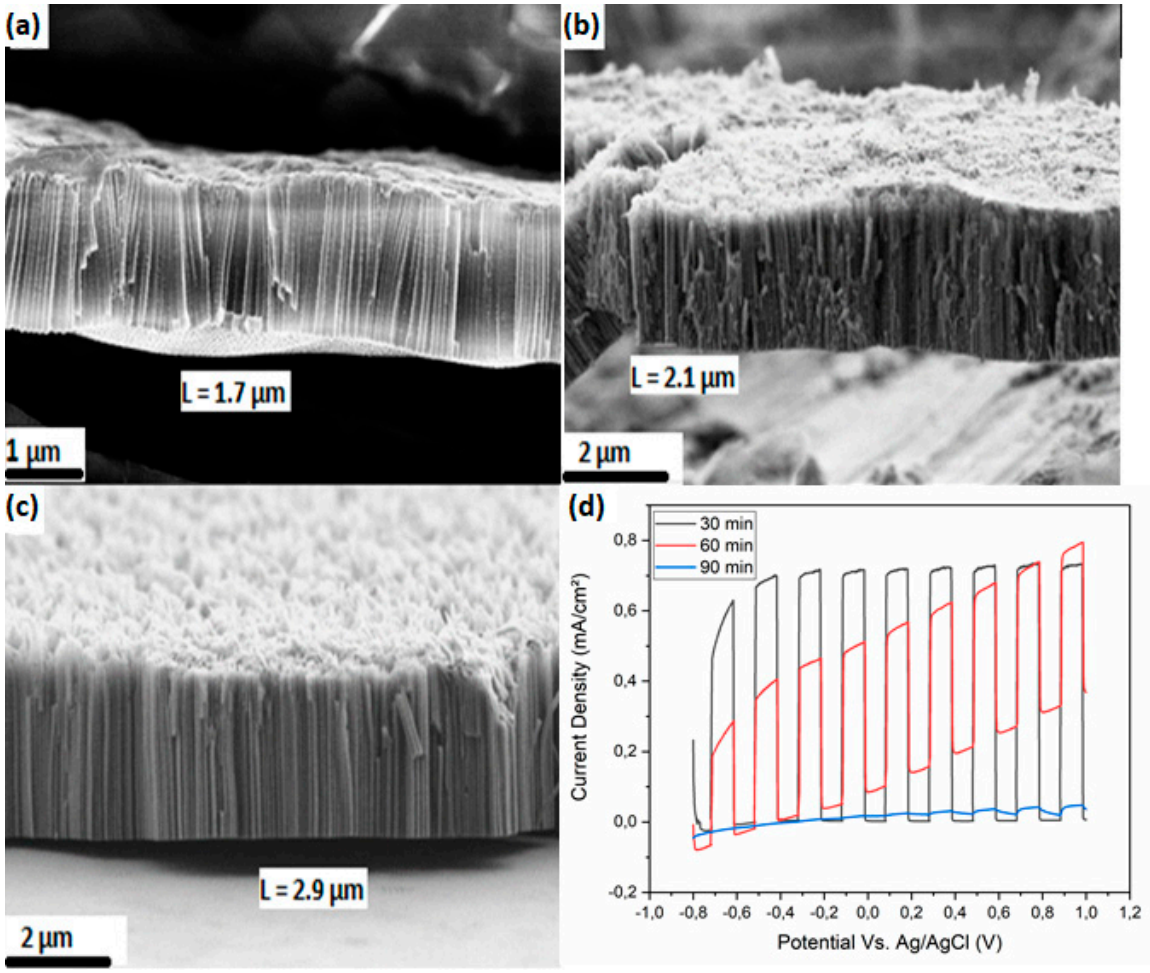

Figure 6. FESEM images of the TiO_2 nanotube arrays under different anodization times: (**a**) 30 min, (**b**) 60 min and (**c**) 90 min. (**d**) Corresponding photocurrent density under different anodization times (samples prepared using constant electrolyte concentration (0.8 wt% NH_4F) and anodization voltage (30 V)).

Previous works have reported that the increase in the TiO_2 tube length provides a larger active surface area, therefore offering higher absorption of the incident light, resulting in more photogenerated electron/hole pairs and therefore improved photoelectrochemical activity [33]. However, our results show that (while keeping the pore opening size constant), the photoelectrochemical properties decrease with increasing tube length (Figure 6d).

Our experimental results can be explained by the increase in the tube layer thickness, which is one of the most influential parameters affecting the photoelectrochemical efficiency of TiO2 nanotubes. The observed decrease in the photoelectrochemical activity of the TiO2 nanotubes with increasing tube length is ascribed to the coating electric conductivity. In fact, the resistivity of the TiO2 nanotubes increases with increasing tube length, resulting in an apparent decrease in the photocurrent density. Moreover, this behavior can also be explained by the light penetration within the nanotubes to photogenerate the electron/hole pairs. In fact, it has been proven by Hitchman et al. [34] that the maximum light penetration depth into TiO2 is the reciprocal of the absorption coefficient of the TiO2 film at the wavelength of the incident light, allowing light penetration up to a maximum depletion layer width (W_{max}). Therefore, any hole generated within W_{max} will be transported to the coating when located in the TiO2 minority carrier diffusion length. On the other hand, absorptions at higher depths will lead to charge recombination [34]. This result is also corroborated by Dosta et al.'s

previous work [35], which reports that the photogeneration of oxidants can be enhanced up to a film thickness limit.

The significant decrease in the photocurrent density (Figure 6d) can be explained by the fact that when the nanotube length is higher, the incident light needs to travel a longer pathway within the TiO_2 tubes, which also explains the decrease in the photoelectrochemical activity due to the high chance of the recombination of the photogenerated electron/hole pairs.

2.4.3. Effect of Anodization Voltage

The effect of the anodization voltage on the photoelectrochemical properties of the prepared TiO_2 nanotubes is investigated by applying different anodization voltages ranging from 15 to 100 V (Figure 7a–f).

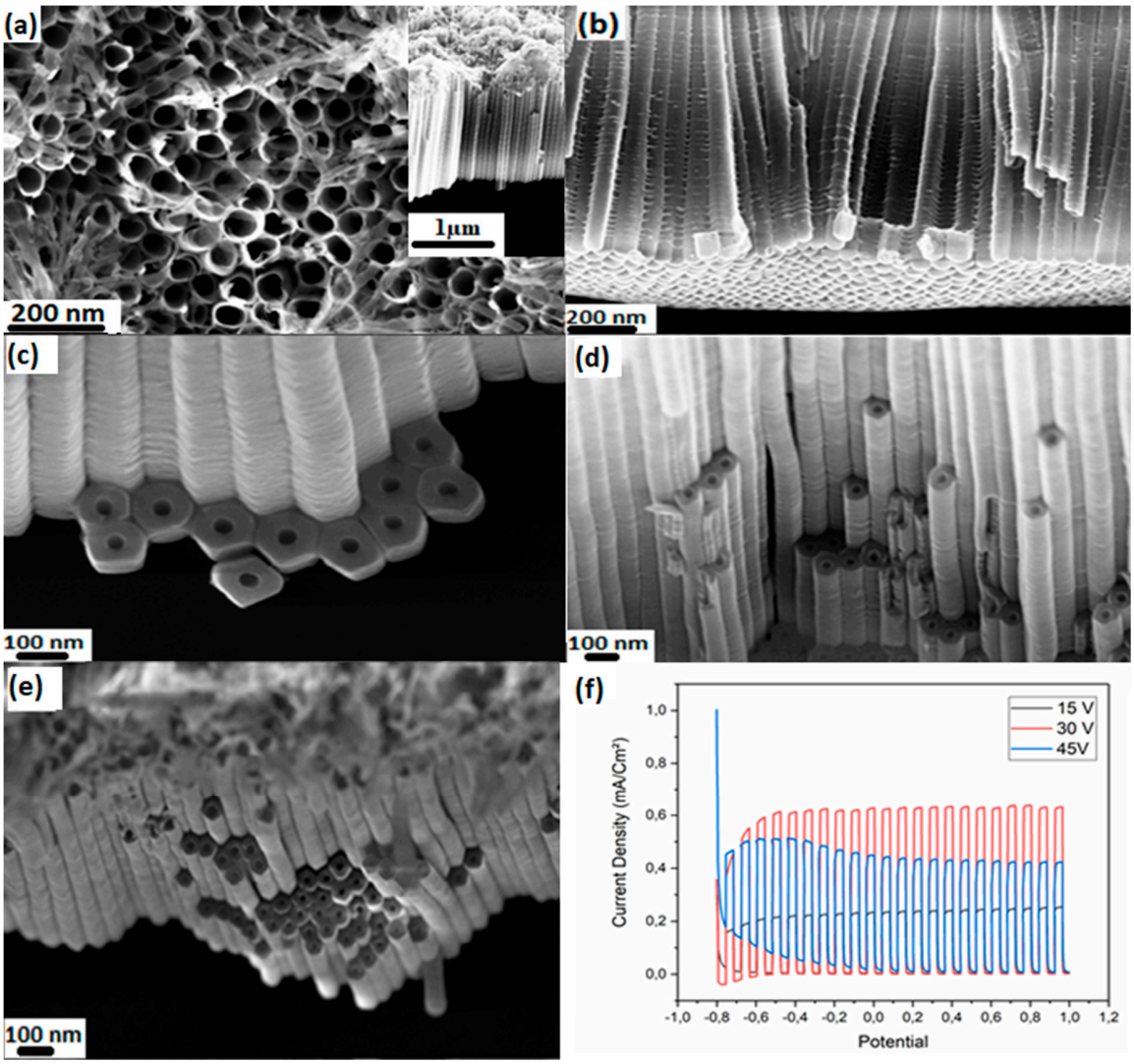

Figure 7. FESEM cross-section images of the TiO_2 nanotubes prepared under different anodization potentials, (**a**) 15, (**b**) 30, (**c**) 45, (**d**) 55 and (**e**) 65 V. (**f**) Current transient of the TiO2 nanotubes prepared under different anodization potentials. (samples prepared using constant electrolyte concentration (0.8 wt% NH_4F) and anodization time (30 min).

The anodization potential plays a key role in the TiO_2 nanotube formation, as their growth results from the attained equilibrium between Ti electrochemical oxidation and TiO_2 chemical dissolution. Therefore, as the anodization potential increases, the anodization current increases, which accelerates the oxidation–dissolution equilibrium and leads to the fine-tuning of the tube wall thickness. According to the FESEM images (Figure 7), it can be observed that both the pore diameter and the tube length of the nanotubes increase with higher applied voltage.

In addition, as depicted in Figure 7a, the TiO_2 nanotubes prepared under 15 V anodization potential (0.8 wt% NH_4F electrolyte, 30 min anodization time) have the lowest tube length (inset of Figure 7a), with small pore openings. This hinders the diffusion of the pollutant or electrolyte solution into the tubes.

Moreover, it can also be observed from Figure 7 that the tubes have a somewhat cone-like structure, showing thinner walls on the upper part of the tube and thicker walls on the bottom. This is explained by higher etching of the fluorine ions on the upper part of the tubes. Therefore, the volume of TiO_2 strongly decreases in the upper part of the tubes, while the tube length increases due to a higher anodization time or anodization potential. Consequently, the light needs to travel a longer pathway within the tubes before it is absorbed and the electron/hole pairs are generated. Additionally, the electrolyte solution has to diffuse further in the tubes, resulting in a photoelectrochemical activity decrease.

Previous results have shown that TiO_2 nanotubes with higher tube lengths in a specific range provide larger active surface areas, and consequently increase the absorption of the incident photons. The photoelectrochemical behavior of TiO_2 nanotubes under different applied anodization potentials is also investigated using the same photoelectrochemical cell, and the results are shown in Figure 7f.

The TiO_2 nanotubes prepared using an anodization potential of 15 V are short and the wall thickness is large (the pore diameter is small), which obstructs the diffusing of the electrolyte/pollutant inside the nanotubes. The tube length is also critical, and needs to be sufficiently long to gain high UV absorption.

It is observed that, with increasing anodization potential, the tubes are longer and the etching rate is higher; thus, the volume of TiO_2 in the walls decreases (the pore diameter is large, see FESEM images in Figure 7). The results show that the photoelectrochemical activity of the tubes decreased, which is due to the fact that the photogenerated electrons have to travel a longer pathway and are prone to recombination with holes. The TiO_2 nanotubes prepared at higher anodization voltage (from 55 to 100 V) were subject to stability issues and were prone to partial peeling off the foil surface. Therefore, the photocurrent response of these tubes was not measured.

In order to further confirm the photocurrent measurement results, and to investigate the working mechanism and the electronic properties of the TiO_2 samples, electrochemical impedance spectroscopy (EIS) analysis was performed to study the impedance and capacitance of the TiO_2 nanotubes in dark conditions and under UV illumination at 365 nm. The Nyquist plots (Figure 8) represent the opposite of the imaginary part of the complex impedance (Z″) as a function of the real part (Z′) and are corroborated by the photoelectrochemical (PEC) tests. As depicted in Figure 8a, the charge transfer resistance recorded for the samples prepared with a higher ammonium fluoride content (1.4 wt% NH_4F) is lower compared to samples anodized at a lower ammonium fluoride content (0.4 wt% NH_4F), which confirms the photocurrent density results presented in Figure 4.

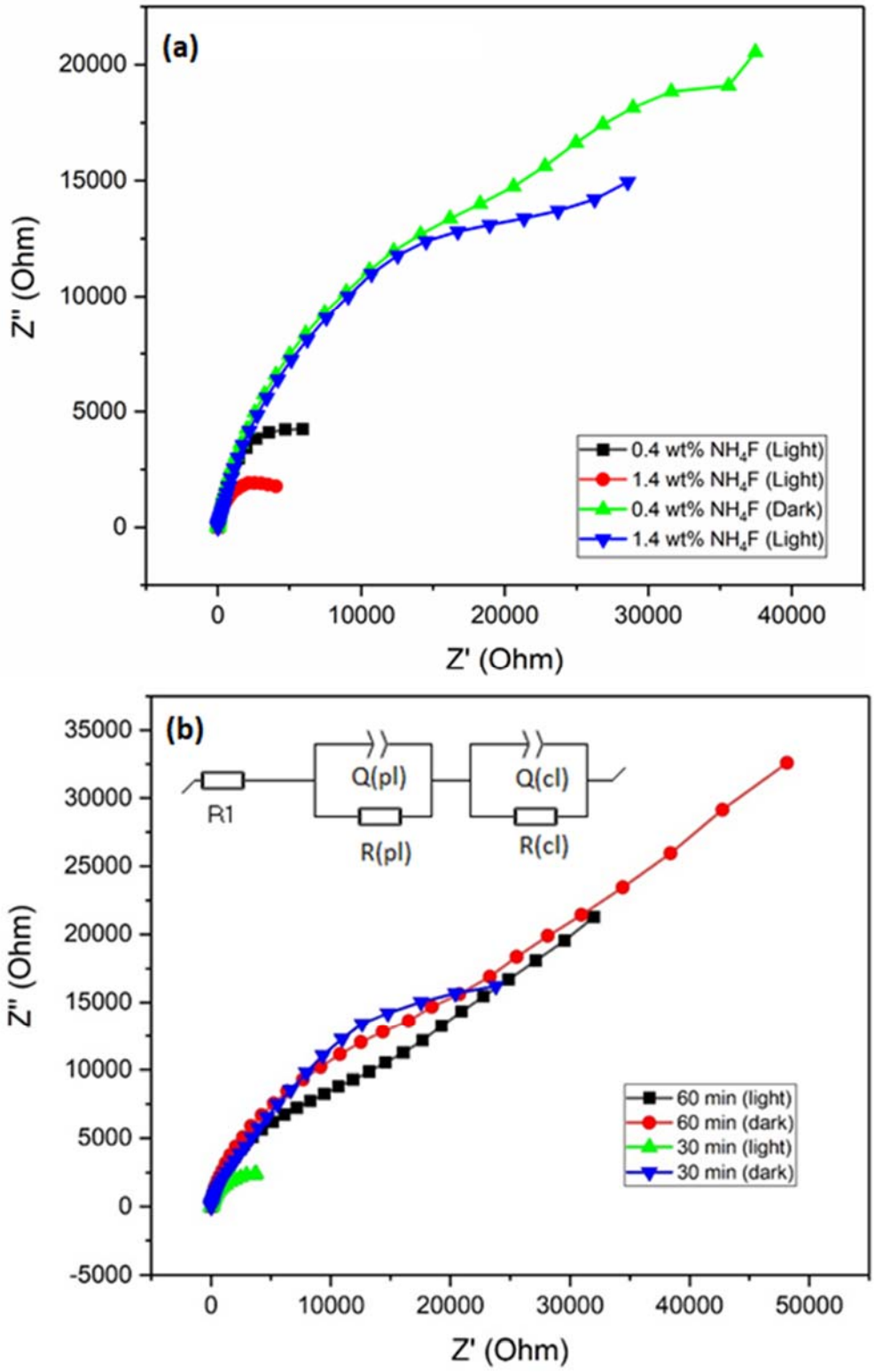

Figure 8. Nyquist plots for measured in the dark and under UV irradiation at 365 nm. (**a**) TiO_2 nanotubes prepared using different ammonium fluoride concentrations. (**b**) TiO_2 nanotubes prepared at different anodization times.

As reported in similar studies [36], the behavior of the TiO_2 nanotubes can be represented by a structure consisting of two layers—a compact base layer and a porous overlayer—where the TiO_2 nanotubes are fully formed (Figure 1). Therefore, two RQ components are needed in the equivalent circuit in order to consider the capacitive–resistive processes taking place at the interface of the two layers (inset of Figure 8b). The RQ circuit component with higher resistance (R_{cl}) is associated with the compact base layer, whereas the behavior of the porous layer, consisting of the fully formed TiO_2 nanotubes, is associated with the RQ components with lower resistances (R_{pl}).

The circuit components obtained from both the compact and the porous layers are shown in Table 1, the values of the resistance R1 are between 14 and 16 Ohm for all samples, which take into account the solution resistance as well as the external resistance. On the other hand, the TiO_2 nanotube samples prepared under different anodization conditions have different surface morphologies and superficial areas, which explain the different values of resistance and capacity, as well as charge distribution.

Table 1. Circuit components calculated by fitting the experimental impedance data.

Sample	R1 [Ω]	Porous Layer			Compact Layer		
		R(pl) [Ω]	C(pl) [F]	τ_{pl} (s)	R(cl) [Ω]	C(cl) [F]	τ_{cl} (s)
TiO2 NT (0.4 wt% NH4F)	16.8	274	1.83E-04	5.01E-02	8573	1.43E-04	1.23E+00
TiO2 NT (1.4 wt% NH4F)	14.27	53.42	3.29E-05	1.76E-03	3806	1.30E-07	4.95E-04
TiO2 NT (30V, 30 min)	14.03	45.67	3.24E-05	1.48E-03	4111	1.48E-04	6.08E-01
TiO2 NT (30V, 60 min)	14	54.74	3.19E-05	1.75E-03	5985	8.34E-05	4.99E-01
TiO2 NT (45V)	15.37	56.81	3.43E-05	1.95E-03	5994	8.37E-05	5.02E-01

As shown in Figure 8b and Table 1, the recorded charge transfer resistance for TiO_2 samples prepared at higher anodization times is higher for both the porous layer and the compact layer, compared to samples prepared at lower anodization times, which confirms the photoelectrochemical results presented in Figure 6d showing lower photocurrent density values. In addition, the TiO_2 samples prepared under 30 V exhibit lower resistance compared to samples prepared under 45 V, which allows a better charge separation and less electron/hole recombination on the nanotubes. This result corroborates the photocurrent results in Figure 7f.

The electron lifetime ($\tau = R \times C$) at the depletion layer of the semiconductor is calculated from the fitted values of resistance and capacitance, and the values are reported in Table 1. As expected, the TiO2 samples exhibiting higher photocurrent densities show a shorter electron lifetime. In fact, the samples prepared with s higher ammonium fluoride content (1.4 wt% NH4F) present a shorter electron lifetime compared to samples anodized at a lower ammonium fluoride content (0.4 wt% NH4F), which infers that the time spent by an electron in the depletion layer is lower, and the charge transfer is faster, reducing the probability of recombination with a hole. These results further confirm the photocurrent density results presented in Figure 4. Likewise, the electron lifetime of TiO_2 samples prepared at higher anodization times is higher compared to the samples prepared at lower anodization times, which is in good agreement with the photoelectrochemical results.

3. Experimental

3.1. Materials

Titanium foil (0.127 mm thick, 99.99+% metals basis) was obtained from Alfa Aesar. Ethylene glycol (≥ 99%, for synthesis) was purchased from CarlRoth GmbH+Co (Karlsruhe, Germany). KG. Ammonium fluoride (for analysis EMSURE® ACS) was obtained from Merck KGaA (Darmstadt, Germany). Palladium foil (99.9%, 1 mm thick) was purchased from ChemPur Feinchemikalien und Forschungsbedarf GmbH (Karlsruhe, Germany). Deionized water was used throughout all experiments and was obtained from a Millipore system with a resistivity of >18.2 MU cm.

3.2. Preparation of TiO_2 Nanotubes

Before the anodization, the titanium foils were degreased by sonicating in acetone, ethanol, and Millipore water, followed by rinsing in Millipore water and blow-drying with nitrogen. The anodization process was carried out at room temperature in a two-electrode electrochemical cell, using the titanium foil as the anode and palladium foil as the cathode. The experiments were performed using an electrolyte solution prepared from ethylene glycol, containing ammonium fluoride (NH_4F) and 3 vol% deionized water.

Before the anodization of the polycrystalline titanium foil, the electrolyte solution was aged by anodizing titanium foil for 2 h [37]. The concentration of the ammonium fluoride present in the electrolyte solution, the anodization time and anodization potential varied, and the anodization current was monitored using a Rigol Digital Multimeter (model 3051). After the anodization process ended, the substrates were kept in in the electrolyte solution for 30 min in order to prevent surface aggregation [37]. To remove the electrolytes from their surfaces, the titanium foils were washed thoroughly with deionized water and subsequently dried under a gentle nitrogen flow.

In order to crystallize the as-prepared amorphous TiO_2 nanotubes, post-annealing treatment was performed at 420 °C for 90 min with a heating and cooling rate of 10 K per minute.

3.3. Characterization Techniques

The morphology of the TiO_2 nanotubes was characterized using a field emission scanning electron microscope (FESEM; Zeiss Ultra 55, Jena, Germany). The X-ray diffraction (XRD) patterns were measured on an Ultima IV X-ray diffraction spectrometer (Rigaku, Tokyo, Japan) with Cu Kα radiation and operated at 40 kV and 40 mA with a scanning speed of 1° min^{-1} at a step size of 0.01°. X-ray photoelectron spectroscopy (XPS) was performed on Axis Ultra (Kratos Analytical Ltd., Manchester, UK) with a monochromatic Al Kα cathode and an X-ray source with 150 W power and 40 eV pass energy.

PEC measurements were performed in a three-electrode configuration in a self-made quartz-windowed Teflon cell. The same Ag/AgCl reference and platinum counter electrodes were used. An AM1.5 solar illumination (100 mW cm^{-2}) with a WACOM super solar simulator (WXS-50S-5H, class AAA) was used as an illumination source. The electrolyte used for all measurements was 1 M KOH with 10 vol% of ethylene glycol added, which acted as a hole scavenger. The potential is converted to the reversible hydrogen electrode (RHE) potential based on the Nernst equation [38,39]:

$$E_{RHE} = E_{Ag/AgCl} + 0.059pH + E^{\circ}_{Ag/AgCl} \quad (7)$$

where E_{RHE} is the converted potential versus the reversible hydrogen electrode, $E_{Ag/AgCl}$ is the measured potential versus the Ag/AgCl reference electrode, and $E^{\circ}_{Ag/AgCl}$ is equal to 0.1976 V at room temperature (~25 °C). The photoelectrochemical behavior of TiO_2 nanotube arrays was determined by linear sweep voltammetry, at a scan rate of 20 mV s^{-1} from −0.8 to 1.0 V (vs. RHE).

Electrochemical impedance spectroscopy (EIS) measurements were carried out with a potentiostat VSP-300 by Biologic. The samples have been measured with 10mV sinus amplitude within a frequency range of 1–100 mHz with 10 points per decade. Every point was measured threefold and averaged. A three-electrode setup was used with platinum counter and reference electrodes. All measurements were carried out in dark conditions and under UV illumination at 365 nm. The used light source was a 30 W UV LED lamp from UVECO, and the average light intensity striking on the surface of the TiO_2 electrodes was measured by a UV-radiometer from Jenoptik (Jena, Germany), and was 40 mW/cm^2.

4. Conclusions

In this work, highly ordered and self-organized TiO_2 nanotube arrays were fabricated using a rapid anodization process, and a systematic study on the impact of electrochemical growth conditions on the TiO_2 nanotubes' geometrical parameters, as well as their photoelectrochemical properties, was carried out. The optimal anodization parameters are demonstrated by means of photocurrent

density measurements and linear sweep voltammetry in order to achieve the most efficient charge carrier separation. It is shown that the length, pore opening and wall thickness critically affect the photoelectrochemical activity of the TiO_2 nanotubes. The photocurrent density decreased with increasing tube length, which was elucidated by higher chances of the electron/hole pair's recombination. Moreover, the charge transfer resistance for longer TiO_2 nanotubes prepared at higher anodization times was higher compared to shorter nanotubes prepared at lower anodization times, which confirms the impact of the nanotube length on the electron lifetime in the depletion layer and on the charge transfer.

Moreover, the lowest photocurrent densities were observed for TiO_2 nanotubes with smaller pore diameter, namely TiO_2 nanotubes prepared using electrolytes with low ammonium fluoride content, as well as TiO_2 prepared under low anodization potential. The corresponding decrease in the photoelectrochemical activity can be explained by the hindered diffusion of the electrolyte solution into the tubes and a higher charge transfer resistance, which therefore decreased the photocurrent density.

The results of the electrochemical impedance spectroscopy (EIS) were correlated with the microstructural characterization and the photocurrents measurements. The combined results allow a better understanding of the electronic properties of TiO_2 nanotubes and the effect of the anodization growth parameters on the tubes' properties, such as the surface morphology, electron charge resistance and electron lifetime.

In order to achieve high photoelectrochemical performance, the nanotubes' geometrical parameters need to be optimized in order to avoid limitations in the charge transport of the TiO_2 photoelectrodes, which can be attained by optimizing the anodization parameters and engineering the morphology of the nanotubes to reduce the chances of the electron/hole pair's recombination.

Author Contributions: Conceptualization and Visualization by H.E. and B.A.; Methodology by H.E., K.F., A.C. and K.H.; J.G. performed the XRD, M.K. performed SEM, and A.P. performed XPS. Resources provided by A.S.; Supervision by B.A.; Project Administration by H.E. and B.A.; Writing of the paper and Funding Acquisition by H.E. All authors have read and agreed to the published version of the manuscript.

Funding: Funding by the Alexander von Humboldt Foundation though a research fellowship to Houda Ennaceri is gratefully acknowledged.

Conflicts of Interest: The authors declare no conflict of interest.

References

1. Fujishima, A.; Honda, K. Electrochemical Photolysis of Water at a Semiconductor Electrode. *Nature* **1972**, *238*, 37–38. [CrossRef]
2. Kalanoor, B.S.; Seo, H.; Kalanur, S.S. Recent developments in photoelectrochemical water-splitting using WO3/BiVO4 heterojunction photoanode: A review. *Mater. Sci. Energy Technol.* **2018**, *1*, 49–62.
3. Zhu, H.; Zhao, M.; Zhou, J.; Li, W.; Wang, H.; Xu, Z.; Lu, L.; Pei, L.; Shi, Z.; Yan, S.; et al. Surface states as electron transfer pathway enhanced charge separation in TiO2 nanotube water splitting photoanodes. *Appl. Catal. B Environ.* **2018**, *234*, 100–108. [CrossRef]
4. Yu, L.; Zhang, Y.; He, J.; Zhu, H.; Zhou, X.; Li, M.; Yang, Q.; Xu, F. Enhanced photoelectrochemical properties of α-Fe2O3 nanoarrays for water splitting. *J. Alloy. Compd.* **2018**, *753*, 601–606. [CrossRef]
5. Ullah, H.; Tahir, A.A.; Bibi, S.; Mallick, T.K.; Karazhanov, S.Z. Electronic properties of β-TaON and its surfaces for solar water splitting. *Appl. Catal. B Environ.* **2018**, *229*, 24–31. [CrossRef]
6. Singh, A.P.; Kodan, N.; Mehta, B.R.; Held, A.; Mayrhofer, L.; Moseler, M. Band Edge Engineering in BiVO4/TiO2 Heterostructure: Enhanced Photoelectrochemical Performance through Improved Charge Transfer. *ACS Catal.* **2016**, *6*, 5311–5318. [CrossRef]
7. Cheng, B.-Y.; Yang, J.-S.; Cho, H.-W.; Wu, J.-J. Fabrication of an Efficient BiVO4–TiO2 Heterojunction Photoanode for Photoelectrochemical Water Oxidation. *ACS Appl. Mater. Interfaces* **2016**, *8*, 20032–20039. [CrossRef]
8. Su, J.; Zhang, T.; Wang, L. Engineered WO_3 nanorods for conformal growth of $WO_3/BiVO_4$ core–shell heterojunction towards efficient photoelectrochemical water oxidation. *J. Mater. Sci. Mater. Electron.* **2017**, *28*, 4481–4491. [CrossRef]

9. Garcia-Segura, S.; Brillas, E. Applied photoelectrocatalysis on the degradation of organic pollutants in wastewaters. *J. Photochem. Photobiol. C Photochem. Rev.* **2017**, *31*, 1–35. [CrossRef]
10. Weon, S.; Choi, J.; Park, T.; Choi, W. Freestanding doubly open-ended TiO2 nanotubes for efficient photocatalytic degradation of volatile organic compounds. *Appl. Catal. B Environ.* **2017**, *205*, 386–392. [CrossRef]
11. Gao, X.; Kong, C.P.; Jia, R.; Jian, W.; Wang, J.; Bai, F.Q.; Zhang, H.X. Influence of one-dimensional TiO2 nanotube on interfacial electron transfer in dye-sensitized solar cells: Insights from theoretical investigation. *Sol. Energy* **2018**, *176*, 545–555. [CrossRef]
12. Zhou, X.; Yu, S.; Guan, S.; Lv, Z.; Liu, E.; Zhao, Y. Fabrication and characterization of superhydrophobic TiO2 nanotube coating by a facile anodic oxidation approach. *Surf. Coat. Technol.* **2018**, *354*, 83–91. [CrossRef]
13. Zhang, Y.; Zhu, H.; Zhuang, C.; Chen, S.; Wang, L.; Dong, L.; Yin, Y. TiO2 coated multi-wall carbon nanotube as a corrosion inhibitor for improving the corrosion resistance of BTESPT coatings. *Mater. Chem. Phys.* **2016**, *179*, 80–91. [CrossRef]
14. Tian, M.; Thind, S.S.; Dondapati, J.S.; Li, X.; Chen, A. Electrochemical oxidation of 4-chlorophenol for wastewater treatment using highly active UV treated TiO2 nanotubes. *Chemosphere* **2018**, *209*, 182–190. [CrossRef] [PubMed]
15. Qiao, H.; Xiao, H.; Huang, Y.; Yuan, C.; Zhang, X.; Bu, X.; Wang, Z.; Han, S.; Zhang, L.; Su, Z.; et al. SiO2 loading into polydopamine-functionalized TiO2 nanotubes for biomedical applications. *Surf. Coat. Technol.* **2019**, *364*, 170–179. [CrossRef]
16. Xun, H.; Zhang, Z.; Yu, A.; Yi, J. Remarkably enhanced hydrogen sensing of highly-ordered SnO2-decorated TiO2 nanotubes. *Sens. Actuators B: Chem.* **2018**, *273*, 983–990. [CrossRef]
17. Hejazi, S.; Nguyen, N.T.; Mazare, A.; Schmuki, P. Aminated TiO2 nanotubes as a photoelectrochemical water splitting photoanode. *Catal. Today* **2017**, *281*, 189–197. [CrossRef]
18. Kumaravel, V.; Mathew, S.; Bartlett, J.; Pillai, S.C. Photocatalytic hydrogen production using metal doped TiO2: A review of recent advances. *Appl. Catal. B Environ.* **2019**, *244*, 1021–1064. [CrossRef]
19. Borbón-Nuñez, H.A.; Dominguez, D.; Muñoz-Muñoz, F.; Lopez, J.; Romo-Herrera, J.; Soto, G.; Tiznado, H. Fabrication of hollow TiO2 nanotubes through atomic layer deposition and MWCNT templates. *Powder Technol.* **2017**, *308*, 249–257. [CrossRef]
20. Liu, N.; Chen, X.; Zhang, J.; Schwank, J.W. A review on TiO2-based nanotubes synthesized via hydrothermal method: Formation mechanism, structure modification, and photocatalytic applications. *Catal. Today* **2014**, *225*, 34–51. [CrossRef]
21. Fischer, K.; Gläser, R.; Schulze, A. Nanoneedle and nanotubular titanium dioxide – PES mixed matrix membrane for photocatalysis. *Appl. Catal. B Environ.* **2014**, *160*, 456–464. [CrossRef]
22. Foong, T.R.B.; Shen, Y.D.; Hu, X.; Sellinger, A. Template-directed liquid ALD growth of TiO2 nanotube arrays: Properties and potential in photovoltaic devices. *Adv. Funct. Mater.* **2010**, *20*, 1390–1396. [CrossRef]
23. Neville, E.M.; MacElroy, J.M.D.; Thampi, K.R.; Sullivan, J.A. Visible light active C-doped titanate nanotubes prepared via alkaline hydrothermal treatment of C-doped nanoparticulate TiO2: Photo-electrochemical and photocatalytic properties. *J. Photochem. Photobiol. A Chem.* **2013**, *267*, 17–24. [CrossRef]
24. Zwilling, V.; Aucouturier, M.; Darque-Ceretti, E. Anodic oxidation of titanium and TA6V alloy in chromic media. An electrochemical approach. *Electrochim. Acta* **1999**, *45*, 921–929. [CrossRef]
25. Zwilling, V.; Darque-Ceretti, E.; Boutry-Forveille, A.; David, D.; Perrin, M.Y.; Aucouturier, M. Structure and Physicochemistry of anodic oxide films on titanium and TA6V alloy. *Surf. Interface Anal.* **1999**, *27*, 629–637. [CrossRef]
26. Suna, Y.; Yan, K.-P. Effect of anodization voltage on performance of TiO2 nanotube arrays for hydrogen generation in at wo-compartment photoelectrochemical cell. *Int. J. Hydrog. Energy* **2014**, *39*, 11368–11375. [CrossRef]
27. Smith, Y.R.; Kar, A.; Subramanian, V.R. Investigation of physicochemical parameters that influence photocatalytic degradation of methyl orange over TiO_2 nanotubes. *Ind. Eng. Chem. Res.* **2009**, *48*, 10268–10276. [CrossRef]
28. Mazzarolo, A.; Lee, K.; Vicenzo, A.; Schmuki, P. Anodic TiO2 nanotubes: Influence of top morphology on their photocatalytic performance. *Electrochem. Commun.* **2012**, *22*, 162–165. [CrossRef]
29. Mariena, C.B.D.; Cottineau, T.; Robert, D.; Drogui, P. TiO2 Nanotube arrays: Influence of tube length on the photocatalytic degradation of Paraquat. *Appl. Catal. B Environ.* **2016**, *194*, 1–6. [CrossRef]

30. Lebedeva, O.; Kultin, D.; Kudryavtsev, I.; Root, N.; Kustov, L. The role of initial hexagonal self-ordering in anodic nanotube growth in ionic liquid. *Electrochem. Commun.* **2017**, *75*, 78–81. [CrossRef]
31. Li, J.; Zhang, Z.Y.; Li, Y.X.; Ma, Y.J.; Chen, L.; Zhang, Z.Y.; Sun, R.G. Self-organization process of aluminum oxide during hard anodization. *Electrochim. Acta* **2016**, *213*, 14–20. [CrossRef]
32. Deen, K.M.; Farooq, A.; Raza, M.A.; Haide, W. Effect of electrolyte composition on TiO2 nanotubular structure formation and its electrochemical evaluation. *Electrochim. Acta* **2014**, *117*, 329–335. [CrossRef]
33. Ku, Y.; Fan, Z.-R.; Chou, Y.-C.; Wang, W.-Y. Characterization and Induced Photocurrent of TiO2 Nanotube Arrays Fabricated by Anodization. *J. Electrochem. Soc.* **2010**, *157*, H671–H675. [CrossRef]
34. Hitchman, M.L.; Tian, F. Studies of TiO2 thin films prepared by chemical vapour deposition for photocatalytic and photoelectrocatalytic degradation of 4-chlorophenol. *J. Electroanal. Chem.* **2002**, *538*, 165–172. [CrossRef]
35. Dosta, S.; Robotti, M.; Garcia-Segura, S.; Brillas, E.; Cano, I.G.; Guilemany, J.M. Influence of atmospheric plasma spraying on the solar photoelectro-catalytic properties of TiO2 coatings. *Appl. Catal. B Environ.* **2016**, *189*, 151–159. [CrossRef]
36. Palmas, S.; da Pozzo, A.; Delogu, F.; Mascia, M.; Vacca, A.; Guisbiers, G. Characterization of TiO2 nanotubes obtained by electrochemical anodization in organic electrolytes. *J. Power Sources* **2012**, *204*, 265–272. [CrossRef]
37. Zhu, W.; Liu, X.; Liu, H.; Tong, D.; Yang, J.; Peng, J. An efficient approach to control the morphology and the adhesion properties of anodized TiO2 nanotube arrays for improved photoconversion efficiency. *Electrochim. Acta* **2011**, *56*, 2618–2626. [CrossRef]
38. Li, Y.; Takata, T.; Cha, D.; Takanabe, K.; Minegishi, T.; Kubota, J.; Domen, K. Vertically Aligned Ta3N5 Nanorod Arrays for Solar-Driven Photoelectrochemical Water Splitting. *Adv. Mater.* **2013**, *25*, 125–131. [CrossRef]
39. Ai, G.; Li, H.; Liu, S.; Mo, R.; Zhong, J. Solar Water Splitting by TiO2/CdS/Co−Pi Nanowire Array Photoanode Enhanced with Co−Pi as Hole Transfer Relay and CdS as Light Absorber. *Adv. Funct. Mater.* **2015**, *25*, 5706–5713. [CrossRef]